Astron. Astrophys. 321, 634–642 (1997)

ASTRONOMY
AND
ASTROPHYSICS

SVD preprocessing of helioseismic data for solar structure inversion

Sarbani Basu[1], **J. Christensen-Dalsgaard**[1,2], **and M.J. Thompson**[3]

[1] Teoretisk Astrofysik Center, Danmarks Grundforskningsfond, Institute for Fysik og Astronomi, Aarhus Universitet, DK-8000 Aarhus C, Denmark
[2] Institute for Fysik og Astronomi, Aarhus Universitet, DK-8000 Aarhus C, Denmark
[3] Astronomy Unit, Queen Mary and Westfield College, Mile End Road, London E1 4NS, UK

Received 30 July 1996 / Accepted 25 September 1996

Abstract. Helioseismic inversion to determine solar structure is based on the analysis of very substantial numbers of modes and hence may involve considerable computational expense. This is particularly true for inversions using methods of optimally localised averages, which require inversion of matrices whose order is the number of modes in the set; yet such methods are desirable to make the full use of the data. On the other hand, there is considerable redundancy in the data, different modes carrying almost the same information about solar structure. Thus, in the unavoidable presence of data errors, the number of independent pieces of information is generally much less than the number of modes. This suggests that the modeset can be reduced by forming suitable combinations of the data before the more computationally intensive inversion is performed. We show that such combinations may be based on singular value decomposition (SVD) of the problem, leading to a drastically reduced inverse problem whose solution is essentially indistinguishable from the solution of the original problem. In addition, the results of the SVD provide insight into the information content of the helioseismic data.

Key words: Sun: oscillations – Sun: interior – methods: data analysis

1. Introduction

Global solar oscillation frequencies can be determined to very high precision. Hence comparison of computed and observed frequencies provides a stringent test of models of the solar interior. In fact, no physical model of the Sun reproduces the observed frequency spectrum at the level of accuracy provided by the observations. As a result, to infer the detailed structure of the Sun the helioseismic data must be inverted.

Send offprint requests to: S. Basu

The observed global oscillations of the Sun are well described throughout most of the solar interior by the equations describing linear adiabatic oscillations. (cf. Unno et al. 1989). These equations, along with appropriate boundary conditions, constitute a self-adjoint eigenvalue problem, which leads to a variational principle connecting the eigenfrequency to the basic equilibrium state. This has been extensively used as the basis for inversions to determine the structure of the Sun (e.g. Gough & Kosovichev 1988, 1993; Dziembowski, Pamyatnykh & Sienkiewicz 1990; Däppen et al. 1991; Antia & Basu 1994; Dziembowski et al. 1994). Such inversions proceed by linearizing the equations of solar oscillations about a known reference model of the Sun. Schematically, we can write our inverse problem as

$$d_i = \int \underline{K}^i(r) \cdot \underline{\delta X}(r)\,\mathrm{d}r + \epsilon_i \,, \tag{1}$$

where d_i is the ith datum, $\underline{K}^i$ is a vector function, the kernel, which is a known function of the reference model, $\underline{\delta X}$ is the unknown vector function for which we wish to invert, and ϵ_i is the error in the ith datum. In our case, d_i is the relative differences between the observed frequency of the ith mode and the corresponding frequency of the reference model (more correctly, the mean multiplet frequency for given radial order and degree, averaged over azimuthal order); $\underline{\delta X}(r)$ is a 2-vector describing the relative structural differences between the Sun and the model relevant for adiabatic oscillations of a spherically symmetric, self-gravitating body in hydrostatic equilibrium; r is the radial coordinate describing position inside the Sun; and the integral runs from the centre of the Sun ($r = 0$) to the surface (taken to be located at the chromospheric temperature minimum).

Various standard linear inversion techniques are available for inverting a set of constraints such as Eq. (1) – see the above references and Sect. 2 below. A characteristic feature of the inverse problem is the very large number of modes available for inversion and the large degree of redundancy in the information they contain (see Christensen-Dalsgaard, Hansen & Thompson 1993). This leads to an ill-posed problem, and unless precau-

tions are taken, errors in the data cause large errors in the solution (e.g. Craig & Brown 1986). To control the errors, trade-off parameters have to be introduced in the inversion techniques, and these must be determined as a part of the solution. This and the large amount of data available in general makes inversion computationally expensive.

It was shown by Christensen-Dalsgaard & Thompson (1993) that in the case of inversion to determine solar rotation, it is possible to exploit the redundancy of the data to reduce the problem at hand. They demonstrated that, by using a singular value decomposition, one can form a new, smaller set of data that are linear combinations of the original data. This smaller set contains all the useful information of the original dataset, and because of its size can be inverted by some standard inversion techniques much more quickly than could the original set. Our purpose in this paper is to demonstrate that similar preprocessing is effective also in the case of the inversion for solar structure.

The essence of the preprocessing is therefore to find a smallish set of linear combinations of the data that contains essentially the same information about the solar interior as the full dataset. This will then be our new transformed dataset. The empirical test to show that all useful information has been retained is that the same inversion solutions and averaging kernels can be derived with the new dataset as with the original one. We can write the new data as

$$\widetilde{d}_i \equiv \sum_j U_{ji} d_j \tag{2}$$

for some coefficients U_{ji}; and since this is just a linear operation it follows from Eq. (1) that

$$\widetilde{d}_i = \int \widetilde{\underline{K}}^i \cdot \underline{\delta X}\, \mathrm{d}r + \widetilde{\epsilon}_i \,, \tag{3}$$

where $\widetilde{\underline{K}}^i$ and $\widetilde{\epsilon}_i$ are the corresponding combinations of the kernels and the errors. The essential point is that the necessary number $\widetilde{M}$ of new data is smaller than the original number M of data, if the coefficients U_{ji} are chosen judiciously.

How then are these coefficients U_{ji} to be determined? The strategy we adopt is to form a matrix, each row of which is a discretized representation of the kernels $\underline{K}^i$, and to find the singular value decomposition (SVD) of that matrix. We then derive the required coefficients from the singular vectors corresponding to the largest, most significant, singular values of the kernel matrix. This is analogous to the approach Christensen-Dalsgaard & Thompson used for the rotation inversion, and is closely related also to methods that have been adopted in other areas of astrophysics for handling large datasets (e.g. Zaroubi et al. 1995; Tegmark et al. 1997).

One difference between inversion for solar rotation and that for solar structure is that in the case of rotation there is only one unknown scalar function, namely the rotation rate, whereas in structure inversion two unknown scalar functions determine the frequency differences, i.e., the two components of vector function $\underline{\delta X}(r)$. These two functions may be, for example, the relative differences in the adiabatic sound speed squared (c^2) and in density ρ; or if, in addition to the assumption of hydrostatic equilibrium the equation of state and heavy element-abundance are assumed known, then the two functions may be e.g. the relative difference in density and the difference in helium abundance Y.

There is a second difference between inversions for rotation and structure. In the latter case, a significant contribution to the frequency differences that constitute the data arises from non-adiabatic effects and other inadequacies of the forward model in the near-surface layers. In the absence of any reliable formulation for these effects, they are taken into account in an *ad hoc* manner by including on the right-hand side of Eq. (1) an additive term:

$$d_i = \int \underline{K}^i(r) \cdot \underline{\delta X}(r)\, \mathrm{d}r + F_{\mathrm{surf}}/E_i + \epsilon_i \,. \tag{4}$$

Fortunately, the surface term cannot be a completely general function of mode parameters. Having factored out the inertia E_i of the mode, the function F_{surf} can be expanded as (cf., Brodsky & Vorontsov 1993; Antia 1995; Gough & Vorontsov 1995)

$$F_{\mathrm{surf}} = F_0(\omega) + \frac{F_1(\omega)}{w^2} + \frac{F_2(\omega)}{w^4} + \cdots, \tag{5}$$

where ω is the angular frequency and $w = \omega/(l + 0.5)$. Provided the degree l of the mode is not too large, all terms except the first can be ignored, i.e., the function F_{surf} is a function of the frequency ω_i but is independent of l. Moreover, it is a relatively slowly varying function of frequency. As a consequence, it is possible to perform a linear projection to remove the surface term and recast the inversion problem into the form (1). Alternatively, it is perhaps simpler (and therefore more commonly done) to work with the full Eq. (4), parametrizing F_{surf} as a low-order polynomial with unknown coefficients which are themselves to be determined or else eliminated as part of the inversion procedure. We adopt the latter approach here, in Sect. 4.

The plan of the rest of the paper is as follows. In Sect. 2 we discuss the setting up and singular value decomposition of the matrix of discretized kernels. It should be borne in mind that the only purpose of discretizing the kernels is to obtain the coefficients for transforming problem (1) to problem (3): this transformation is performed in Sect. 3, and the results of inversions with transformed and full datasets are compared. For clarity, we exclude the possibility of a near-surface term F_{surf} in Sects. 2 and 3. In Sect. 4 we indicate how things are modified in the presence of F_{surf}, and we consider the effect of more realistic errors in the data in Sect. 5.

2. Discretization and SVD of the matrix of kernels

In this section and the next, we neglect the surface term F_{surf}, so that the full inverse problem is described by Eq. (1). Approximating each component of $\underline{\delta X}$ in terms of basis functions $\phi_k(r)$,

$$\underline{\delta X}(r) = \sum_k \begin{pmatrix} b_k \\ c_k \end{pmatrix} \phi_k(r) \,, \tag{6}$$

the integral term on the right of Eq. (1) can be replaced by a matrix product $A\mathbf{x}$, where the elements of $\mathbf{x}$ are the b_k and c_k. If there are M modes in the set (i.e., M data), and there are N basis functions ϕ_k, then A is an $M \times P$ matrix where $P = 2N$. The elements of matrix A are:

$$A_{ij} = \begin{cases} \int_0^{R_\odot} K_1^i \phi_j(r)\mathrm{d}r \ , & \text{if } j \le P/2 \ , \\ \int_0^{R_\odot} K_2^i \phi_{j-P/2}(r)\mathrm{d}r \ , & \text{if } P/2 < j \le P \ , \end{cases} \tag{7}$$

where K_1^i and K_2^i are the two components of the vector $\underline{K}^i$ in Eq. (1). The matrix A can be written in terms of its singular value decomposition (SVD)

$$A = U\Sigma V^{\mathrm{T}}, \tag{8}$$

where Σ is a diagonal matrix containing the singular values $\{\sigma_i\}$ of A ($\sigma_1 \ge \sigma_2 \ge \sigma_3 \ge \cdots$), U (of order $M \times P$) and V (of order $P \times P$) are orthonormal matrices, with the property that $U^{\mathrm{T}}U$ and $V^{\mathrm{T}}V = VV^{\mathrm{T}}$ are equal to an identity matrix.

We now show the results of applying the procedure above to a test example. Following Antia & Basu (1994) we define a set of points $0 \equiv r_0 < r_1 < r_2 \cdots < r_{N-1} \equiv R_\odot$ in the interval [0,$R_\odot$], distributed equally in acoustic depth τ. Then our basis functions $\phi_k(r)$ are defined to be the cubic B-spline basis functions over r centred at the knots r_k; these are normalized to a maximum value of unity so that, roughly, c_k and d_k are of the magnitude of the corresponding component of $\underline{\delta X}(r_k)$.

We expect the results of the SVD to be similar for kernels from any modern standard solar model. However, to be specific, let us note that for the following numerical results we have used model S of Christensen-Dalsgaard et al. (1996). The model was constructed with OPAL opacities (Iglesias, Rogers & Wilson 1992), and with the OPAL equation of state (Rogers, Swenson & Iglesias 1996). It incorporates gravitational settling of helium and other heavy elements, and has an age of 4.6 Gyr. This model is also the reference model of the inversion in subsequent sections. The results will depend more on the modeset used. We have used all modes from the first year of observations by the LOWL instrument (Tomczyk et al. 1995) except for 24 modes with unusual characteristics, such as much lower errors or linewidths than neighbouring modes. The set consists of 1130 modes of degrees 0 to 99 in the frequency range 1–3.5 mHz (Schou, Tomczyk & Thompson 1996; Schou & Tomczyk 1997). In this section and the next two we assume uniform uncertainties on the data: we relax this assumption in Sect. 5.

First we consider the effect of the discretization on the spectrum of singular values of matrix A. We choose $\underline{\delta X} \equiv (\delta \ln c^2, \delta \ln \rho)$ as our unknown variables. Fig. 1 shows the singular value spectrum for different numbers N of radial knots. Except when very few knots are used, there is a plateau of about one hundred singular values, beyond which the singular values rapidly become much smaller. A similar behaviour was seen in the case of rotation (Christensen-Dalsgaard et al. 1993), though there the plateau of high singular values was rather flatter than in the present case. The behaviour as the number of knots is increased is qualitatively similar in the two cases. Provided a sufficient number of knots is used, the large singular values are

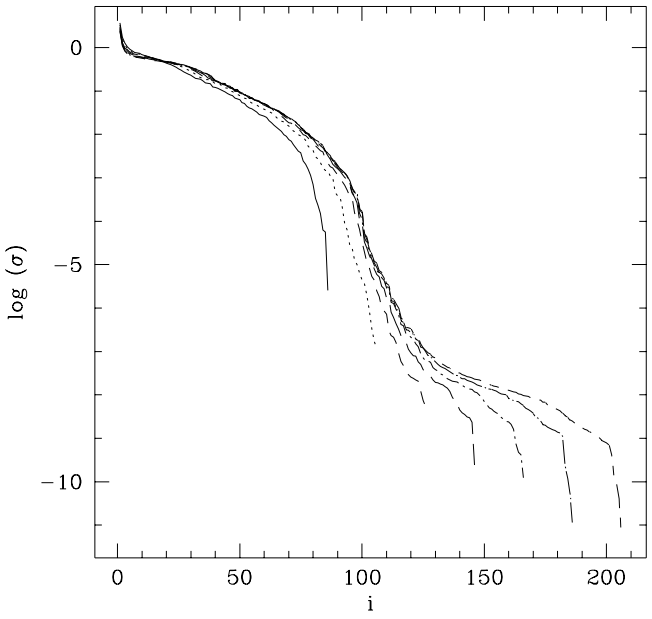

Fig. 1. The singular value spectrum of the matrix A as defined in Eq. (7), when the variable combination of (c^2, ρ) is used. The points are joined together for the sake of clarity. Shown are the spectra for 41 knots in r (continuous line), 51 knots (dotted line), 61 knots (short-dashed line), 71 knots (long-dashed line), 81 knots (dot-short dashed line), 91 knots (dot-long dashed line) and 101 knots (short dash-long dashed line)

essentially independent of N. These SVD components represent the significant information about solar structure contained in the modeset. Indeed, the minimum-norm regularized least-squares solution to the inverse problem can essentially be obtained from the components corresponding to the largest singular values, truncating the expansion at a level which depends on the errors in the data (e.g. Hanson 1971; Christensen-Dalsgaard et al. 1993). Potential information from components corresponding to small singular values will in practice be inaccessible because of data errors. The smallest singular values are probably dominated by round-off errors. With our discretization and modeset, 61 knots seem just about adequate to capture the behaviour of the plateau of large singular values correctly. For 71 or more knots the spectrum appears to reach the round-off error limit. Thus we believe that a minimum of about 70 knots in radius are required. For the rest of the paper, we use 81 knots in r.

To investigate further the correspondence between the structural SVD and that for the rotation kernels, we have computed the singular value spectra using just one component of the kernels, i.e., corresponding to just one of the unknown variables. Fig. 2 shows that the spectrum for sound-speed kernels alone does have a flatter plateau, terminated by a well defined shoulder, which is very similar to the spectrum for rotation kernels. The spectrum for density kernels alone is quite similar. Thus the less well-defined plateaux in Fig. 1 are in some sense a consequence of having the two variables at once. However, we note that at a given index i, σ_i for the combined case is similar to, but slightly larger than, the value obtained for c^2 alone. It is perhaps

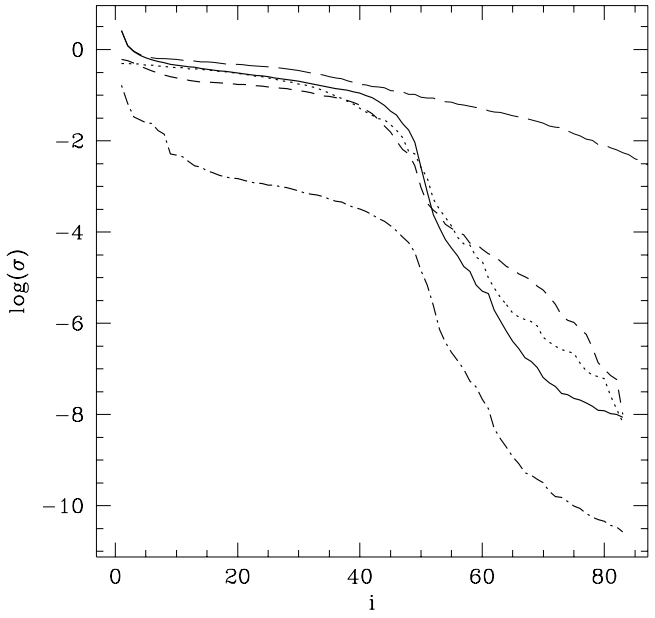

Fig. 2. The singular value spectrum of just the c^2 kernels at constant ρ (continuous line), the ρ kernels at constant c^2 (dotted), the ρ kernels at constant helium abundance Y (dashed), and the Y kernels at constant ρ (dot-dashed). In all cases, 81 knots were used. For comparison, the long-dashed line shows the corresponding singular values obtained with the variable combination (c^2, ρ)

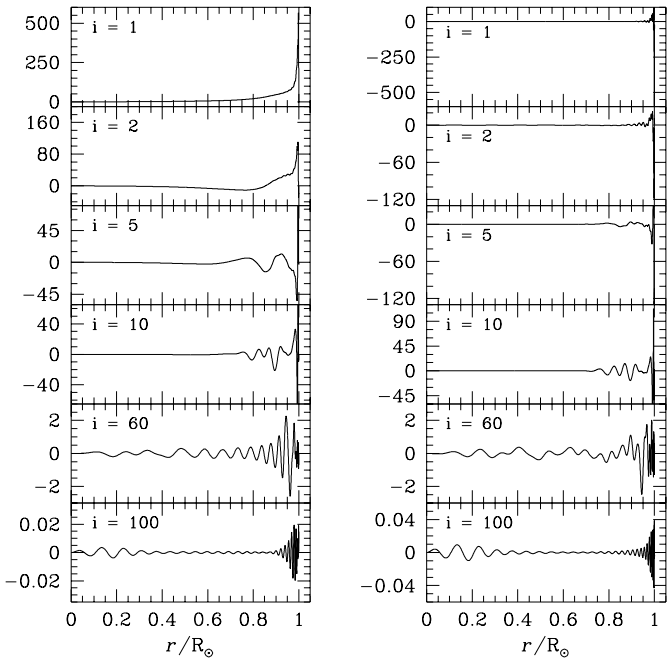

Fig. 3. A sample of the transformed kernels, obtained using 81 knots in r. The panel on the left are the transformed sound-speed kernels, while those on the right are the transformed kernels for density

not surprising that inversion for two variables allows extraction of a larger number of significant components of the solution, and hence leads to a more extended spectrum of comparatively large singular values, although at the expense of the less sharply defined transition to small singular values. It is interesting also that the largest few singular values in the combined case are virtually identical to those for c^2; the same is true of the corresponding components of the U and V matrices. This indicates that the most well-determined components of the solution in the combined case are associated with sound speed, as might indeed have been anticipated.

Other pairs of variables can be used, and Fig. 2 shows also the spectra for individual variables from another choice of variable pair: $\underline{\delta X} \equiv (\delta \ln \rho, \delta Y)$. Once again the spectra exhibit well-defined plateaux, of similar length. However, we note that the singular values for δY are much reduced relative to the others, except for the first few, reflecting the difficulty in obtaining detailed information about the helium abundance except in the dominant ionization zones of hydrogen and helium.

3. OLA inversion of the transformed problem

The ultimate purpose of performing the discretization and SVD in Sect. 2 is to find out what suitable linear combinations of the original data will provide a smaller set of transformed data and yet retain the useful information in the original dataset. Guided by rotation inversions (Christensen-Dalsgaard & Thompson 1993), we take the elements U_{ji} from the matrix of left singular vectors as our coefficients U_{ji} in the transformation of Eq. (1) to Eq. (3). With the singular values ordered to be monotonic decreasing, we expect that we can just take the columns of U (i.e., the index i) corresponding to the largest singular values. Applying this transformation yields transformed kernels

$$\widetilde{\underline{K}}^i = \sum_{j=1}^{M} U_{ji} \underline{K}^j, \quad i = 1, \cdots, \widetilde{M}. \tag{9}$$

Corresponding to the singular values in Fig. 1, we show in Fig. 3 a few of the transformed kernels for squared sound speed and density. As in the case of rotation, the transformed kernels are increasingly oscillatory as i increases. Also, it is only for moderately large i that the transformed kernels are sensitive to structure in the deep interior, reflecting the fact that this region is relatively inaccessible to p modes. This is the reason why inversion at the core is often so difficult.

After deciding on the discretization used for the SVD, we still have considerable freedom in choosing the number $\widetilde{M}$ of transformed kernels to retain for the subsequent inversion. To assess how large $\widetilde{M}$ has to be to capture essentially all of the useful information in the full dataset, we compare inversions based upon the full and transformed sets of kernels, retaining different numbers of transformed kernels. We use a subtractive optimally localized averages (SOLA) inversion in all cases, since this is an example of an inversion method where it would be attractive to reduce the computational burden by means of the proposed transformation. As in the previous section, for now we do not consider the effect of a surface term.

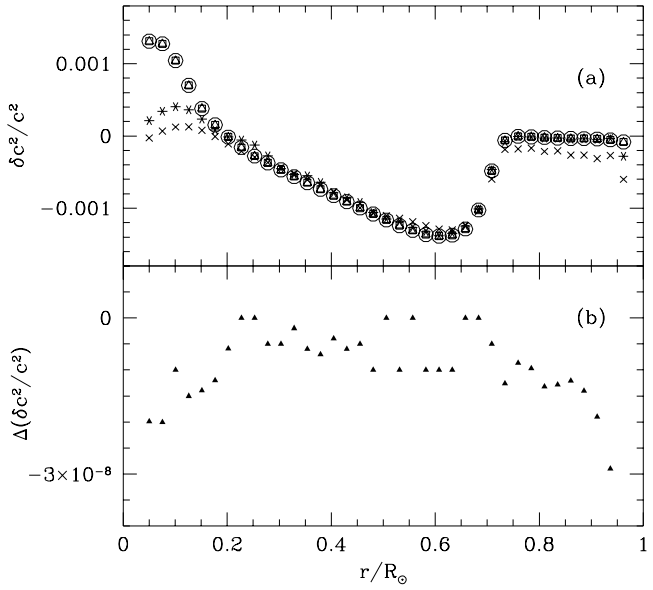

Fig. 4. a The inversion results obtained from the equations transformed with 81 knots in r compared with those obtained from the full set of kernels; results for the latter case are shown with circles. The crosses are for a transformation including 60 singular values, the asterisks for are 80 singular values, the triangles are for 100 singular values and the squares are for 120 singular values. **b** The difference in the inversion results between the solution with the full modeset and those obtained using 120 singular values

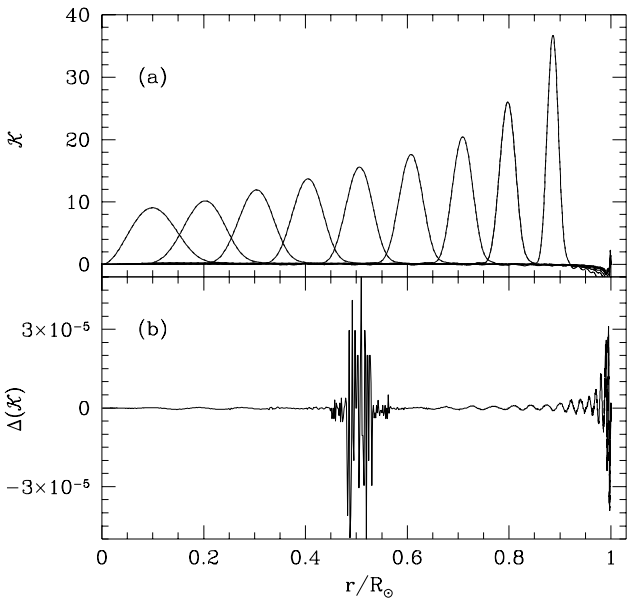

Fig. 5. a Averaging kernels produced by inversion of the full modeset. **b** The difference, for a target radius of $0.5R_\odot$, between the averaging kernel shown in panel **a** and the corresponding kernel for the transformed set with 81 knots and $\widetilde{M}$ = 120

The application of the SOLA method to structural inversions was described by Christensen-Dalsgaard & Thompson (1995). In brief, the aim is to choose coefficients $c_i(r_0)$ such that (say) the first component of $\sum c_i(r_0)\underline{K}(r)$ is localized about $r = r_0$: then provided the other component is small, the corresponding linear combination of the data is a localized estimate of the first component of $\underline{\delta X}(r)$ around $r = r_0$. In SOLA, we choose the coefficients to minimize

$$\int \left(\sum_i c_i K_1^i - \mathscr{T} \right)^2 \mathrm{d}r + \beta \int \left(\sum_i c_i K_2^i \right)^2 \mathrm{d}r + \mu \sum_{i,j} c_i c_j C_{ij} \ , \tag{10}$$

where $\mathscr{T}$ is a chosen target function (here a Gaussian), β is a parameter which controls the influence of the second function on the solution obtained for the first function, μ is a trade-off parameter which controls the error magnification, and C_{ij} is the error covariance matrix for the data. (Although we are here assuming the errors to be uncorrelated and have uniform standard deviations, C_{ij} will usually have a more general form.) The minimization of Eq. (10) is constrained by the requirement that the averaging kernel

$$\mathscr{K}(r_0, r) \equiv \sum c_i(r_0) K_1^i(r) \tag{11}$$

be unimodular.

By way of illustration, we invert artificial data comprising frequency differences between our reference model and a test model. The physics of the test model is similar to that in the reference model, but it is younger, with an age of 4.52 Gyr. Fig. 4 shows the inferred difference in squared sound speed obtained with the original set of kernels (circles) and with various sets of transformed kernels, using 81 knots for the discretization. For $\widetilde{M}$ = 60, the resulting $\delta c^2/c^2$ is somewhat different; for $\widetilde{M}$ = 80 there are still noticeable differences in the core. With further increase in values of $\widetilde{M}$, the differences between the inversions rapidly become imperceptible on this scale. For $\widetilde{M}$ = 120, for example, the differences in the inferred values of sound speed are only a few parts in 10^8.

As a further diagnostic test, we may consider the averaging kernels. Panel (a) of Fig. 5 shows selected averaging kernels obtained in the complete inversion. If the corresponding averaging kernels obtained by inverting the first 120 transformed kernels were plotted on the same scale, the two sets of averaging kernels would be indistinguishable. Thus, for example, panel (b) shows the difference at a target radius of $r_0 = 0.5R_\odot$ between the averaging kernel obtained by inverting the first 120 transformed kernels and the result of the complete inversion: the differences are at the level of 10^{-5}. This provides further evidence that the set of 120 transformed kernels contains essentially the same information as the full set for this inversion.

4. The effect of the surface term

Thus far, we have neglected the surface term F_{surf} which is certainly present when comparing observed frequencies with the frequencies of present-day solar models. As explained in

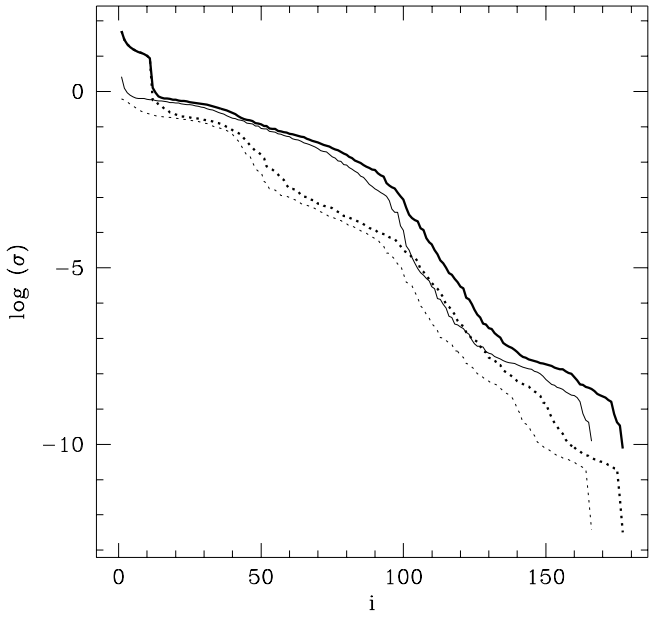

Fig. 6. The singular value spectrum for matrix A as defined in Eq. (12) (thick continuous line) when the variable combination (c^2, ρ) is used. Also shown is the spectrum for the case $\underline{\delta X} = (\delta \ln \rho, \delta Y)$ (thick dotted). For comparison we also show the spectra without the surface terms — thin continuous line for (c^2, ρ), and thin dotted line for $\underline{\delta X} = (\delta \ln \rho, \delta Y)$ In all cases 81 radial knots are used. We have expanded the surface term in Legendre polynomials of degree between 0 and 10

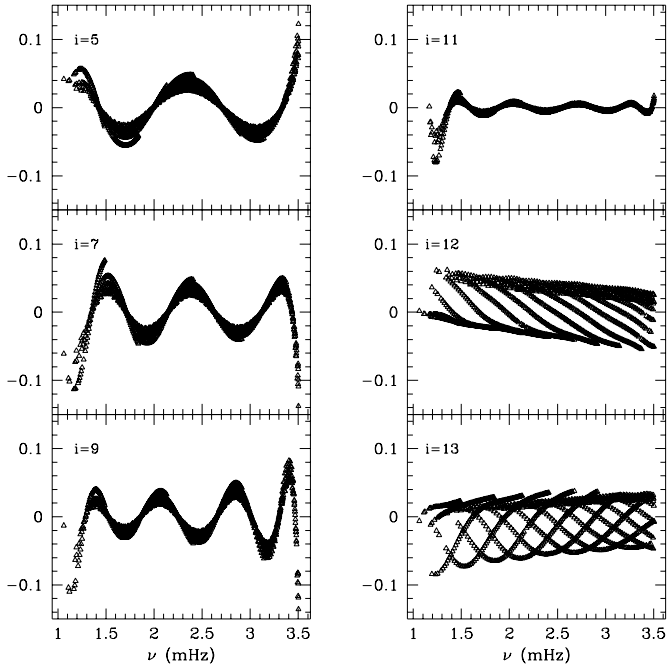

Fig. 7. Some columns of the matrix U, obtained by the decomposition of the matrix A defined in Eq. (12), plotted against cyclic frequency $\nu = \omega/2\pi$

Sect. 1, this term arises from near-surface errors in the model and mode physics, and introduces an extra term in Eq. (4) compared with Eq. (1). To the level of approximation we consider here, the function $F_{\rm surf}$ depends on frequency only.

There are two differences in the way in which we transform and invert data in the presence of the surface term. First, the SVD is based on a discretization that includes the surface term as well as the integral contribution from the kernels. We assume that $F_{\rm surf}(\omega)$ can be expanded in terms of a set of basis functions $\Phi_\lambda(\omega)$ ($\lambda = 1, \cdots, \Lambda$). Then the new matrix A is of order $(M \times P)$, where $P = 2N + \Lambda$, and A has elements

$$A_{ij} = \begin{cases} \int_0^{R_\odot} K_1^i \phi_j(r) \mathrm{d}r \ , & \text{if } j \le N \ , \\ \int_0^{R_\odot} K_2^i \phi_{j-N}(r) \mathrm{d}r \ , & \text{if } N < j \le 2N \ , \\ \Phi_{j-2N}(\omega_i)/Q_i \ , & \text{if } 2N < j \le P \ . \end{cases} \tag{12}$$

Here we have replaced the inertia E_i in Eq. (4) by the inertia ratio $Q_i = E_i/\bar{E}_0(\omega_i)$, where $\bar{E}_0(\omega)$ is the inertia of a radial mode at frequency ω; thus Q_i is of order unity, at least for modes of low or moderate degree (e.g. Christensen-Dalsgaard & Berthomieu 1991). We take the Φ_λ to be proportional to Legendre polynomials, such that $\Phi_\lambda(\omega)$ is between -1 and 1, with suitably scaled argument (cf. Däppen et al. 1991). In Fig. 6, the singular values of this matrix are compared with those of the matrix given by Eq. (7), where the surface term was not taken into account.

The change in the singular-value spectra due to the inclusion of the surface term is quite striking. The main difference seems to be some comparatively large singular values in the case with the surface term. These are undoubtedly due to the extra basis functions of frequency in Eq. (12). One way to gauge the nature of the extra singular values is to look at the corresponding columns of the matrix U. For the singular values that arise due to the surface terms, U_{ji} is expected to be a function of the frequency of the jth mode. Singular vectors associated with the interior of the model, on the other hand, are predominantly functions of the turning point of the mode, which can be represented by w (see also Christensen-Dalsgaard et al. 1993). In the present case we find that the first 11 columns of U are indeed essentially functions of frequency and hence correspond to the basis functions of frequency. The rest are largely functions of w. A few such columns are shown in Fig. 7. Note the qualitatively different behaviour for $i \le 11$ and for $i > 11$. We remark also that the addition of the singular values associated with the surface term causes a shift in the remaining singular values, as seen in Fig. 6.

The second difference in approach in the presence of a surface term is in the OLA inversion itself. Evidently, the linear combination of data of the form (4) will produce an extra term in Eq. (3), which becomes

$$\widetilde{d}_i \ = \ \int \underline{\widetilde{K}}^i \cdot \underline{\delta X} \, \mathrm{d}r \ + \ \sum_j U_{ji} F_{\rm surf}(\omega_j)/E_j \ + \ \widetilde{\epsilon}_i \ . \tag{13}$$

To find the coefficients c_i for the inversion problem in Eq. (4), we minimize Eq. (10) subject to the condition in Eq. (11), and

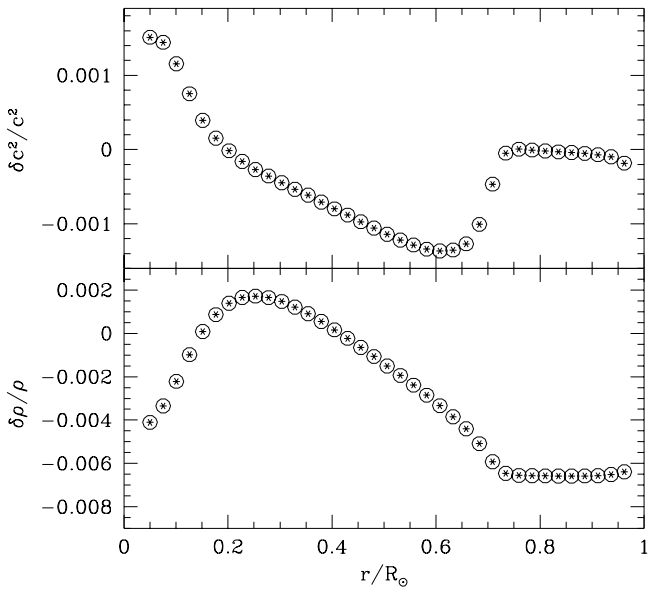

Fig. 8. A comparison of the inversion results of the full modeset (circles) and the transformed set with 81 knots and using 130 singular values (asterisks). The top panel shows the inversion for squared sound-speed, where the second variable is density. The lower panel shows the inversion for density (the second variable being helium abundance). Note that the results for full and transformed sets are virtually indistinguishable

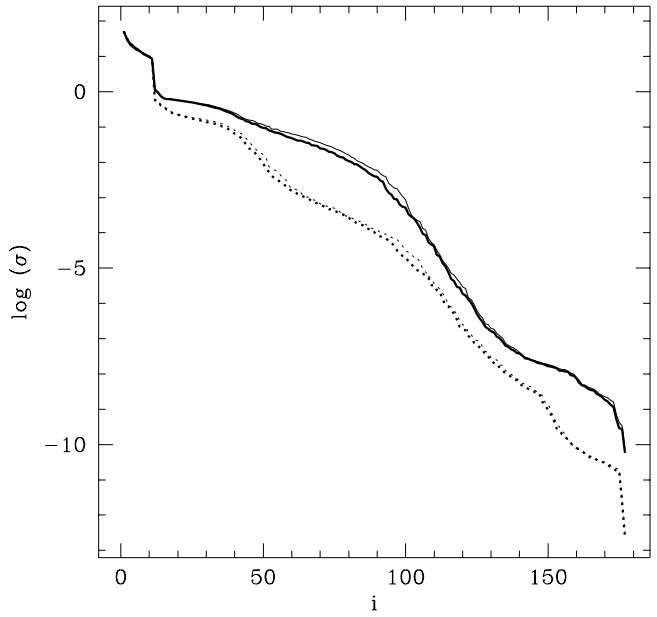

Fig. 9. Singular value spectra for realistic uncertainties in the data. The thick continuous line shows the spectrum when the variable combination (c^2, ρ) is used, while the spectrum for the case $\underline{\delta X} = (\delta \ln \rho, \delta Y)$ is shown as a thick dotted line. For comparison we also show the spectra with uniform errors — thin continuous line for (c^2, ρ), and thin dotted line for $\underline{\delta X} = (\delta \ln \rho, \delta Y)$. In all cases 81 radial knots and 11 surface terms have been used

apply the additional constraints

$$\sum_i c_i(r_0) Q_i^{-1} \Phi_\lambda(\omega_i) = 0 \ , \quad \lambda = 0, \ldots, \Lambda \ . \tag{14}$$

In the transformed case we do something completely analogous, imposing the constraints

$$\sum_i c_i(r_0) \left(\sum_j U_{ji} Q_j^{-1} \Phi_\lambda(\omega_j) \right) = 0 \ , \quad \lambda = 0, \ldots, \Lambda \ . \tag{15}$$

The inversion results are shown in Fig. 8, where we again compare the results obtained by inverting the full modeset and those found by inverting the preprocessed modeset. Whereas without a surface term transformation with 120 singular values was sufficient to reproduce the original solution (cf. Fig. 4), we find that 130 singular values are required once the surface term is included. This increase evidently corresponds approximately to the number of singular values associated with the surface term.

5. The effect of realistic errors

Having investigated the uniform-error case, we turn our attention to a more realistic case in which the errors are still assumed to be independent and Gaussian-distributed, but with individual standard deviations s_i as estimated for LOWL observational 1-year data (Schou et al. 1996; Schou & Tomczyk 1997). As in Sect. 4 we include the effects of a surface term. As a first step, for each datum d_i we renormalize by dividing through Eq. (1) by $s_i/\bar{s}$, where $\bar{s}$ is some typical magnitude for the errors. This renormalizes the data and the kernels in such a way as to give once again a problem in which the errors have identical standard deviations. The factor $\bar{s}$ is included simply to avoid rescaling the kernels by a large factor. After renormalization, the problem looks formally identical to the one we have already considered. We proceed in exactly the same way with the SVD, constructing the transformed kernels and data and performing the SOLA inversion.

The singular value spectrum for the case with realistic errors is shown in Fig. 9. For comparison, we also show the spectrum for the uniform-error case. The factor $\bar{s}$ was chosen so as to make the value of the largest singular value the same in the case of non-uniform errors as in the uniform-error case. In this example, the spectra of singular values in the case of realistic errors are very similar to those for uniform errors. The reason for this is that for this modeset, which only extends up to 3.5mHz, there is not a great range in the quoted uncertainties on the frequencies. There would probably be more substantial differences if higher-frequency data, which are generally less certain, were included. There are differences between the two spectra for intermediate i, with the uniform-error singular values being higher than those for the non-uniform case. This probably reflects the fact that the most deeply penetrating (i.e., low-degree) modes have higher than average uncertainties, so that it is more difficult to invert for the deep interior, relative to the outer envelope, if the data have realistic errors.

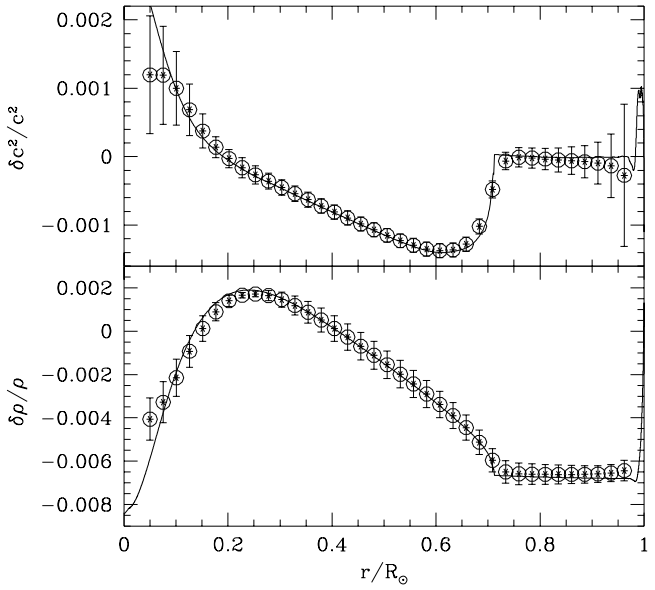

Fig. 10. Comparison of inversion results for the full modeset (circles) and the transformed set using 130 singular values (asterisks). The continuous lines are the exact model differences. The upper panel shows the inversion for squared sound speed, where the second variable is density. The lower panel shows the inversion for density (the second variable being helium abundance). Note that the results for full and transformed sets are virtually indistinguishable. The error bars show propagated errors for the full set; the errors for the transformed set are virtually the same

The inversion results are shown in Fig. 10, where we again compare the results obtained by inverting the full modeset, and those by inverting the preprocessed modeset. As we can see again, $\widetilde{M}$ = 130 and a discretization with 81 knots gives very good results. The propagated errors in the two inversions are essentially identical at each point. Moreover, as we have seen earlier (cf. Fig. 5), the averaging kernels (and hence the resolution) are the same in both inversions. Fig. 10 also shows the exact differences between the test and reference models, thus demonstrating that the inversions do indeed do a good job of estimating the true differences.

6. Conclusions

We have investigated the feasibility of preprocessing a set of solar mean multiplet frequencies before performing inversions for solar structure. This is achieved through forming a linear combination of the original data, with weights obtained from a singular value decomposition of a discretized form of the inverse problem. The inversion is then carried out on only those combinations of modes which correspond to the largest singular values. This enables a reduction of the computational time required for the inversion by a substantial factor — for inversion with optimally localized averages the reduction factor is of the order $(M/\widetilde{M})^3$, where M is the original number of modes and $\widetilde{M}$ the number of combinations included. We have shown that the inversion results, including averaging kernels and propagated errors, obtained with and without the transformations are indeed virtually indistinguishable, provided a sufficient number of combinations are included. In the case considered here the required $\widetilde{M}$ is approximately an order of magnitude smaller than M; thus the saving in computing time is very considerable. The computational effort in setting up the singular value decomposition is modest. Thus for all but the smallest modesets, it is more efficient to preprocess the problem prior to inversion.

The properties of the singular values and associated singular vectors are related to the information content and other aspects of the inverse problem under consideration. For the simple case of rotational inversion in one dimension this was explored in detail by Christensen-Dalsgaard et al. (1993). We have considered a few features of the considerably richer problem of structure inversion, but more detailed investigations of this nature are evidently required. Such investigations would contribute to improving further the efficiency of the inversion procedures, and might provide a deeper insight into the information contents of inversions using different combinations of variables. However, the present investigation has already demonstrated the considerable gain in computational efficiency that can be achieved with SVD preprocessing.

Acknowledgements. This work was supported in part by the Danish National Research Foundation through its establishment of the Theoretical Astrophysics Center and by the UK Particle Physics and Astronomy Research Council through grant GR/J36440.

References

Antia H.M., 1995, MNRAS 274, 499
Antia H.M., Basu S., 1994, A&AS 107, 421
Brodsky M.A., Vorontsov S.V., 1993, ApJ 409, 455
Christensen-Dalsgaard J., Berthomieu G., 1991, In: Cox A.N., Livingston W.C., Matthews, M (eds.) Solar Interior and Atmosphere. Space Science Series, University of Arizona Press, Tuscon, p. 401
Christensen-Dalsgaard J., Thompson M.J., 1993, A&A 272, L1
Christensen-Dalsgaard J., Thompson M.J., 1995, In: Ulrich R.K., Rhodes Jr. E., Däppen W. (eds.) Proc. GONG'94: Helio- and Asteroseismology from Earth and Space. PASPC, 74, 144
Christensen-Dalsgaard J., Hansen P.C., Thompson M.J., 1993, MNRAS 264, 541
Christensen-Dalsgaard J., Däppen W, Ajukov S.V., et al., 1996, Science 272, 1286
Craig I.J.D., Brown J.C., 1986, Inverse problems in astronomy: a guide to inversion strategies for remotely sensed data. Adam Hilger, Bristol.
Däppen W., Gough D.O., Kosovichev A.G., Thompson M.J., 1991, In: Gough D.O., Toomre J. (eds.) Challenges to theories of the structure of moderate-mass stars. Springer, Heidelberg, p. 111
Dziembowski W.A., Pamyatnykh A.A., Sienkiewicz R., 1990, MNRAS 244, 542
Dziembowski W.A., Goode P.R., Pamyatnykh A.A., Sienkiewicz R., 1994 ApJ, 432, 417
Gough D.O., Kosovichev A.G., 1988, In: Domingo V., Rolfe E.J. (eds.), Seismology of the Sun and Sun-like Stars. ESA SP-286, Noordwijk, p. 195
Gough D.O., Kosovichev A.G., 1993, MNRAS 264, 522

Gough D.O., Vorontsov S.V., 1995, MNRAS 272, 573
Hanson R.J., 1971, SIAM J. Numer. Anal. 8, 616
Iglesias C.A., Rogers F.J., Wilson B.G., 1992, ApJ 397, 717
Rogers F.J., Swenson F.J., Iglesias C.A., 1996, ApJ 456. 902
Schou J., Tomczyk S., 1997, in preparation
Schou J., Tomczyk S., Thompson M.J., 1996, Bull. Astron. Soc. India 24, 375
Tegmark M., Taylor A., Heavens A., 1997, ApJ, in press [astro-ph/9603021]
Tomczyk S., Streander K., Card G., Elmore D., Hull H., Cacciani A., 1995, Sol. Phys. 159, 1
Unno W., Osaki Y., Ando H., Shibahashi H., 1989, Nonradial Oscillations of Stars, 2nd Edition. University of Tokyo Press, Tokyo
Zaroubi S., Hoffman Y., Fisher K.B., Lahav O., 1995, ApJ 449, 446

This article was processed by the author using Springer-Verlag LaTeX A&A style file *L-AA* version 3.